Tau accumulation induces synaptic impairment and memory deficit by calcineurin-mediated inactivation of nuclear CaMKIV/CREB signaling

Yaling Yin[a,1], Di Gao[a,1], Yali Wang[a], Zhi-Hao Wang[a], Xin Wang[a], Jinwang Ye[a], Dongqin Wu[a], Lin Fang[a], Guilin Pi[a], Ying Yang[a], Xiao-Chuan Wang[a], Chengbiao Lu[b], Keqiang Ye[c], and Jian-Zhi Wang[a,d,2]

[a]Department of Pathophysiology, School of Basic Medicine and the Collaborative Innovation Center for Brain Science, Key Laboratory of Ministry of Education of China for Neurological Disorders, Tongji Medical College, Huazhong University of Science and Technology, Wuhan 430030, China; [b]Department of Physiology and Neurobiology, Henan Province Key Laboratory of Brain Research, Xinxiang Medical University, Xinxiang 453003, China; [c]Department of Pathology and Laboratory Medicine, Emory University School of Medicine, Atlanta, GA 30322; and [d]Co-Innovation Center of Neuroregeneration, Nantong University, Nantong JS 226001, China

Edited by Solomon H. Snyder, The Johns Hopkins University School of Medicine, Baltimore, MD, and approved May 10, 2016 (received for review March 18, 2016)

Intracellular accumulation of wild-type tau is a hallmark of sporadic Alzheimer's disease (AD), but the molecular mechanisms underlying tau-induced synapse impairment and memory deficit are poorly understood. Here we found that overexpression of human wild-type full-length tau (termed hTau) induced memory deficits with impairments of synaptic plasticity. Both in vivo and in vitro data demonstrated that hTau accumulation caused remarkable dephosphorylation of cAMP response element binding protein (CREB) in the nuclear fraction. Simultaneously, the calcium-dependent protein phosphatase calcineurin (CaN) was up-regulated, whereas the calcium/calmodulin-dependent protein kinase IV (CaMKIV) was suppressed. Further studies revealed that CaN activation could dephosphorylate CREB and CaMKIV, and the effect of CaN on CREB dephosphorylation was independent of CaMKIV inhibition. Finally, inhibition of CaN attenuated the hTau-induced CREB dephosphorylation with improved synapse and memory functions. Together, these data indicate that the hTau accumulation impairs synapse and memory by CaN-mediated suppression of nuclear CaMKIV/CREB signaling. Our findings not only reveal new mechanisms underlying the hTau-induced synaptic toxicity, but also provide potential targets for rescuing tauopathies.

Alzheimer's disease | tau | calcineurin | Ca^{2+}/calmodulin-dependent kinase IV | CREB

Alzheimer's disease (AD) is the most common neurodegenerative disorder characterized clinically by progressive memory loss (1). The extracellular precipitation of β-amyloid (Aβ) (2), intracellular tau accumulation forming neurofibrillary tangles (3), and profound synapse degeneration are hallmark pathologies in AD brains (4, 5). Studies show that formation of neurofibrillary tangles is positively correlated with the degree of dementia symptoms (6), and the Aβ toxicity needs the presence of tau (7). These data suggest a crucial role of tau accumulation in neurodegeneration and the cognitive impairments in patients with AD. As a cytoskeleton protein, how tau accumulation causes memory deficits is not fully understood.

Synapse is the fundamental unit for learning and memory. Dysfunction of synaptic connections is recognized as the cause of memory impairments, and significant synapse loss has been observed in mild cognitive impairment (MCI) and in earlier stages of AD (8). In AD mouse models, synapse impairments appear before the onset of memory deficit (9), whereas amelioration of synapse loss by administration of estradiol preserves cognitive functions (10). Earlier investigations into AD-related synaptic damages have been mainly focused on the toxic effects of Aβ (11). Recently, an emerging role of tau in synaptic impairment has been shown (12). For instance, overexpression of human mutant tau in mice induces synaptic degeneration even in the absence of tangles (13, 14) and reducing endogenous tau in mouse models carrying the mutated amyloid precursor protein (APP) prevents the cognitive deficits and synaptic loss (15).

Among many structural or functional proteins involved in synapse development and memory formation, cAMP response element binding protein (CREB) is one of the most extensively studied (16, 17). CREB is a transcription factor that can regulate the syntheses of synapse- or memory-associated proteins (18, 19). The activity of CREB is regulated by phosphorylation and dephosphorylation, and dephosphorylation disrupts the activity-transcription coupling of CREB in the nuclei (20). Level of the phosphorylated CREB at Ser133 is significantly decreased in the AD hippocampus (21), and knockdown of CREB in mouse brain causes progressive neurodegeneration in hippocampus and the dorsolateral striatum (22). Several kinases can phosphorylate CREB, such as protein kinase A (PKA) (23), mitogen-activated protein kinase (MAPK) (24), protein kinase C (PKC) (25, 26), and calcium/calmodulin-dependent protein kinases (CaMKs) (27). Among various CaMKs, CaMKIV is known to phosphorylate CREB in the nuclei (28, 29). On the other hand, CREB can be dephosphorylated by protein phosphatase 1 (PP1) and calcineurin (CaN, also termed PP2B) (30, 31). In Tg2576 mice, the immunoreactivity

Significance

Memory deterioration is a characteristic clinical symptom in patients with Alzheimer's disease (AD); however, the mechanisms underlying the memory loss are poorly understood. Here, we found that intraneuronal tau accumulation, the hallmark pathology seen in AD brains, induced a remarkable dephosphorylation/inactivation of nuclear cAMP response element binding protein (CREB), an important memory-associated protein. Further studies demonstrated that the abnormal tau accumulation could activate calcineurin, a calcium/calmodulin-dependent protein phosphatase and cause CREB dephosphorylation. Importantly, simultaneous inhibition of calcineurin remarkably attenuated tau-induced CREB inactivation and memory deficits. These findings not only reveal new mechanisms underlying AD memory deficits, but also provide a potential drug target for arresting tauopathies.

Author contributions: Y. Yin and J.Z.W. designed research; Y. Yin, D.G., Y.W., Z.H.W., X.W., J.Y., D.W., L.F., and G.P. performed research; Y. Yin, D.G., Y.W., Y. Yang, X.C.W., C.L., K.Y., and J.Z.W. analyzed data; and Y. Yin and J.Z.W. wrote the paper.

The authors declare no conflict of interest.

This article is a PNAS Direct Submission.

[1]Y. Yin and D.G. contributed equally to this work.

[2]To whom correspondence should be addressed. Email: wangjz@mails.tjmu.edu.cn.

This article contains supporting information online at www.pnas.org/lookup/suppl/doi:10.1073/pnas.1604519113/-/DCSupplemental.

of the phosphorylated CREB was reduced and it was restored by treatment with FK506 (32). In the nuclear fraction of AD brains, a cleaved fragment of CaN (cCaN) is increased and the cleavage activates the phosphatase (33). It is not reported whether and how the human wild-type full-length tau (hereafter, hTau) accumulation may affect these synapse- or memory-related proteins.

By AAV-delivered overexpression of hTau in mouse hippocampus and in cultured hippocampal neurons, we find in the present study that overexpression of hTau in hippocampal neurons induces synapse impairment and memory deficits. The accumulation of hTau inactivated nuclear CaMKIV-CREB signaling by activating CaN, and simultaneous inhibition of CaN effectively arrested the hTau-induced CREB inactivation and rescued the synapse in morphology and the functions with improvement of the memory capacity.

Results

Overexpression of hTau in Hippocampal Neurons Induces Memory Deficits with Dendrite Impairment and Synaptic Dysfunction. To explore the role of hippocampal tau accumulation, an early marker of the AD brain in spatial learning and memory, we injected stereotaxically the AAV-eGFP-hTau into the dorsal hippocampal CA3 of 2-mo-old mice. After 6 wk, the expression of hTau, enriched in hippocampal CA3, was confirmed by immunofluorescence imaging (Fig. 1*A*) and Western blotting using human tau-specific antibody HT7 (Fig. 1*B*). By Morris water maze (MWM) and fear conditioning tests, we observed that the mice with hTau overexpression show significantly increased latency to find the hidden platform during the 6-d learning process compared with the vector controls (Fig. 1*C*), suggesting impairment of special learning by hTau. On day 8, the spatial memory was tested by removing the platform. A remarkably increased latency to reach the platform area with decreased target platform crossings and time in target quadrant was shown in hTau-expressing mice (Fig. 1 *D–F*), suggesting spatial memory deficits. After a 1-wk rest, contextual memory was measured by fear conditioning. The data show that overexpression of hTau decreased freezing time during the 3-min memory test done at 24 h (Fig. 1*G*) or 26 h (Fig. 1*H*) after the training, which confirm the memory impairment by overexpressing hTau.

Previous studies show that overexpression of human mutant tau proteins impairs synapses (14, 34). We found that overexpression of hTau significantly decreased spine density both in hippocampal neurons cultured for 12 d in vitro (div) (Fig. 2 *A–D*) and in vivo measured by Golgi staining (Fig. 2 *E* and *F*). By whole-cell patch-clamp recordings, we recorded spontaneous excitatory postsynaptic currents (sEPSCs) and spontaneous inhibitory postsynaptic currents (sIPSCs) in hippocampal slices (Fig. 2*G*). The hTau accumulation significantly decreased the average frequency of the sEPSCs (Fig. 2*H*) with no significant effects on the average amplitude (Fig. 2*I*) and the average amplitude and frequency of sIPSCs (Fig. 2 *J* and *K*), implying that the hTau accumulation impairs excitatory synaptic transmission in hippocampus. By ex vivo brain slice electrophysiological recording, we found that hTau accumulation suppressed basal synaptic transmission as shown by input–output (IO) curve (Fig. 2*L*) and attenuated the slope of field excitatory postsynaptic potential (fEPSP) after high-frequency stimulation (HFS) (Fig. 2 *M* and *N*). These data together demonstrate that hTau accumulation in hippocampal neurons induces memory deficits with the mechanisms involving structural and functional impairments of the synapses.

Overexpression of hTau Inactivates Nuclear CREB with Up-Regulation of CaN and Inhibition of CaMKIV. To explore the molecular mechanisms that may underlie synapse and memory impairments, we measured CREB, a crucial functional protein for memory formation and consolidation (35). We found that overexpression of hTau in hippocampal neurons cultured for 12 div remarkably decreased the phosphorylation level of CREB at Ser133, although

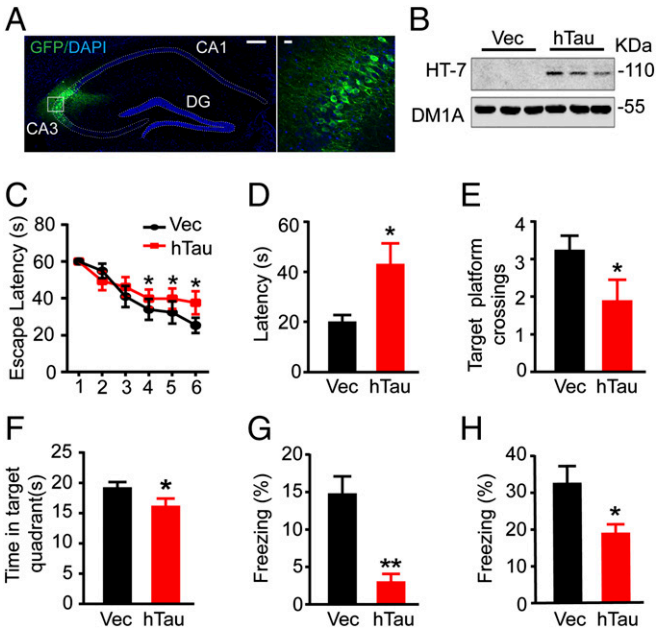

Fig. 1. Tau accumulation in the hippocampal CA3 region impairs learning and memory. (*A*) The representative immunofluorescence imaging of hippocampus and the enlarged CA3 subset after infusion of AAV-eGFP-hTau for 6 wk. [Scale bars: 200 μm (*Left*) and 20 μm (*Right*).] (*B*) Expression of hTau in hippocampal CA3 was confirmed by Western blotting using human tau-specific antibody HT7. (*C*) The escape latency to find the hidden platform in MWM during 6-d learning process. (*D–F*) The escape latency to find the hidden platform, the target platform crossings, and the time spent in the target quadrant measured on day 8 by removing the platform. (*G*) After a 1-wk rest, fear conditioning was used to measure the contextual memory: the mice were exposed to foot shocks for 2 s (0.8 mA) followed by an auditory cue. After 24 h, the mice were put into the same training chamber without shocks and the auditory cue, and the total freezing time in 3 min was recorded with a video camera. (*H*) Two hours later, the freezing time in 3 min was measured again by putting the mice back into the same chamber with the auditory cue for 30 s. Data were expressed as mean ± SEM, $*P < 0.05$, $**P < 0.01$ vs. vector (Vec).

the total CREB was elevated in neuronal lysates (Fig. 3 *A* and *B*). Because the nuclear activity of CREB determines its function (20), we then measured the changes of CREB in the nuclear fraction. We found that the level of phospho-CREB (pCREB) was also significantly decreased with an impaired nuclear translocation in hTau-expressing neurons (Fig. 3*C*). Further studies demonstrated that the dephosphorylation/inactivation of CREB was also significant in mouse hippocampal CA3 after in situ overexpression of hTau (Fig. 3 *I* and *J*). These in vitro and in vivo data indicate that the hTau accumulation induces CREB inactivation.

To explore the mechanisms underlying the hTau-induced CREB dephosphorylation, we first measured the expression level and/or the activity-dependent modifications of protein phosphatases (PPs), including CaN, PP2A, and PP1. We found that overexpression of hTau increased the total level and the cleaved CaN-A (cCaN-A) and CaN-B with an increased biochemical activity of CaN in both lysates and the nuclear fractions (Fig. 3 *D* and *F*); simultaneously, an enhanced nuclear translocation of CaN-B was detected by immunofluorescent staining (Fig. 3*H*). However, overexpression of hTau inhibited PP2A activity shown by the increased demethylation at Leu309 (deM-PP2A) and phosphorylation at tyrosine-307 (pY-PP2A), with reduction of PP1 catalytic subunit in the nuclear fraction (Fig. 3 *L–N*). These data indicate down-regulation of PP2A and PP1 by hTau expression, which exclude the role of these two phosphatases in enhanced CREB dephosphorylation. We also measured CaMKIV (Fig. 3 *D*, *E*, *I*, and *J*) and ERK

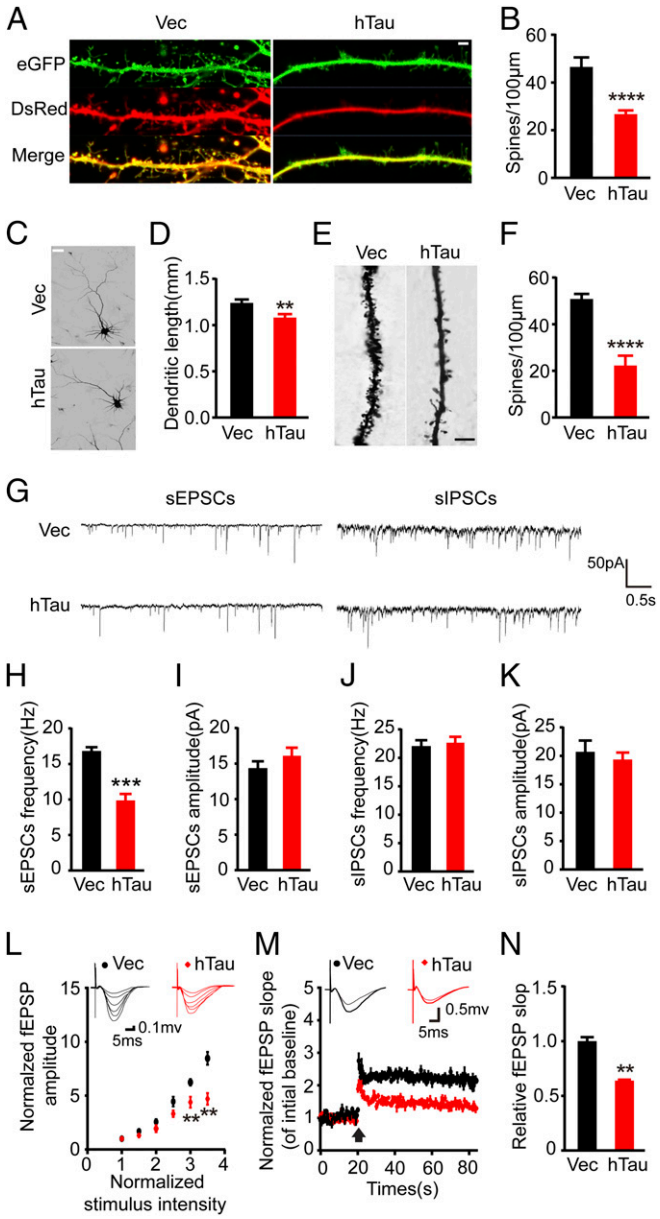

Fig. 2. Overexpression of hTau decreases spine density and the dendrite length with impaired synapse transmission. (*A*) The representative images showing spine density in primary hippocampal neurons (12 div). cotransfection with DsRed and eGFP-hTau (hTau) or DsRed and eGFP (Vec) for 48 h, the images were visualized by using two-photon confocal laser scanning microscopy. (Scale bar, 2 μm.) (*B*) Quantitative analysis of the spine numbers (at least 30 neurons from three independent cultures were analyzed for each group). (*C* and *D*) The primary hippocampal neurons were probed by anti–MAP-2 and the dendrite length was analyzed by Image-pro plus, at least 30 neurons from three independent cultures were analyzed for each group). (Scale bar, 20 μm.) (*E*) The spine density in hippocampal CA3 with overexpression of hTau or the vector measured by Golgi stain. (Scale bar, 10 μm.) (*F*) Quantitative analysis of the spine numbers (at least 15 neurons, three dendritic branches per neuron, from three mice were used for the analysis). (*G*) The representative traces of sEPSCs and sIPSCs measured by whole-cell voltage patch-clamp recording on ex vivo brain slices. (*H–K*) Quantitative analyses of the sEPSC and sIPSC. (*L*) The IO curve of the fEPSP in CA3-CA1, normalized by fEPSP amplitude induced by minimum stimulation intensity. (*M*) The slope of fEPSP after HFS, normalized by the baseline. Arrow indicates the onset of HFS, the traces are average fEPSPs from five sweeps before (thin) and after (thick) LTP induction. (*N*) Quantitative analyses for fEPSPs measured 60–80 min after HFS relative to baseline. Data were expressed as mean ± SEM, $*P < 0.05$, $**P < 0.01$, $***P < 0.001$, $****P < 0.0005$ vs. Vec.

(Fig. 3 *L* and *N*), which can phosphorylate CREB (36). We observed that the nuclear pCaMKIV decreased with a reduced nuclear translocation, although a remarkably increased pCaMKIV was detected in the total lysates (Fig. 3*G*), whereas the activity of ERK was not changed (Fig. 3 *L* and *N*). These data together indicate that CaN activation and/or CaMKIV inhibition are involved in the hTau-induced CREB dephosphorylation in the nuclear fraction.

We observed that levels of total CaMKIIα and p-CaMKIIα and total CaMKIIβ were significantly increased, whereas CaMKIIγ was not changed in lysates; in the nuclear fraction, p-CaMKIIα significantly increased with reduced total CaMKIIα and CaMKIIβ and unchanged CaMKIIγ in hTau-overexpressing cells (Fig. S1). These data, together with the previous reports regarding the role of CaMKII in CREB phosphorylation (37) and the characteristic subtype-specific nuclear translocation of the kinase (38, 39), show that CaMKII may not contribute to CREB dephosphorylation.

As the nuclear factor of activated T cell (NFAT) and GSK-3β are recognized substrates of CaN (40, 41), we also measured these proteins. The total NFAT level was not changed in lysate but significantly increased in the nuclear fraction with a reduced NFAT phosphorylation at serine and threonine residuals measuring immunoprecipitation using NFAT antibody and Western blotting using antiphosphoserine/threonine (Fig. S2). Dephosphorylation of NFAT stimulates its nuclear translocation (42); these data strongly suggest that overexpressing hTau induces NFAT dephosphorylation by CaN activation. Meanwhile, the level of pS9GSK-3β was also decreased in total lysate and the nuclear fractions (Fig. S2 *A–C*), suggesting GSK-3β activation by overexpressing hTau. The result is consistent with a previous report (43) and excludes the role of GSK-3β in CREB dephosphorylation.

CaN Inhibition Attenuates hTau-Induced CREB Dephosphorylation Independent of Its Effect on CaMKIV Inactivation. To further verify the role of CaN and CaMKIV in hTau-induced CREB dephosphorylation, we first used CaN inhibitors FK506 (Fig. 4 *A* and *B*) or cyclosporine A (CsA) (Fig. 4 *C* and *D*) to treat the primary hippocampal neurons (12 div) for 12 h. We found that simultaneous inhibition of CaN could attenuate hTau-induced CREB dephosphorylation with restoration of pCaMKIV level. To further verify whether CaN can directly dephosphorylate CREB or through regulating CaMKIV, we expressed CaMBP4 (a nuclear calmodulin-binding peptide, which blocks nuclear Ca^{2+} signaling) or CaMKIVK75E (a dominant negative mutant of CaMKIV) during CaN inhibition in hTau-overexpression cells. We found that blocking CaMKIV by CaMKIVK75E but not by CaMBP4 further reduced CREB phosphorylation; however, simultaneous inhibition of CaN remarkably restored the pCREB level compared with CaMKIV inhibition alone (Fig. 4 *E* and *F*). These data suggest that CaN can dephosphorylate CREB independent of CaMKIV inactivation. We also observed that simultaneous inhibition of CaN increased the pS9GSK-3β level in both lysate and the nuclear fractions with an increased total GSK-3β and a slight decrease of NFAT in nuclear fraction (Fig. S3). These data confirm the role of CaN in dephosphorylating pS9GSK-3β and NFAT.

Simultaneous Inhibition of CaN Attenuates the hTau-Induced Memory Deficits with Improvement of Synaptic Plasticity and Functions. To validate whether inhibition of CaN could rescue cognitive functions, we injected stereotaxically AAV-eGFP-hTau into the dorsal hippocampal CA3 of 2-mo-old mice. After 45 d, FK506 (10 mg·kg·d) was injected intraperitoneally for 1 wk. Then learning and memory were measured by MWM (Fig. 5 *A–E*) or fear conditioning (Fig. 5 *F* and *G*). We observed that simultaneous inhibition of CaN by intraperitoneal injection of FK506 efficiently rescued hTau-induced memory deficits compared with the vehicle control mice. By ex vivo brain slice electrophysiological recording, we observed that simultaneous inhibition of CaN restored hTau-induced synaptic transmission by increasing the frequency

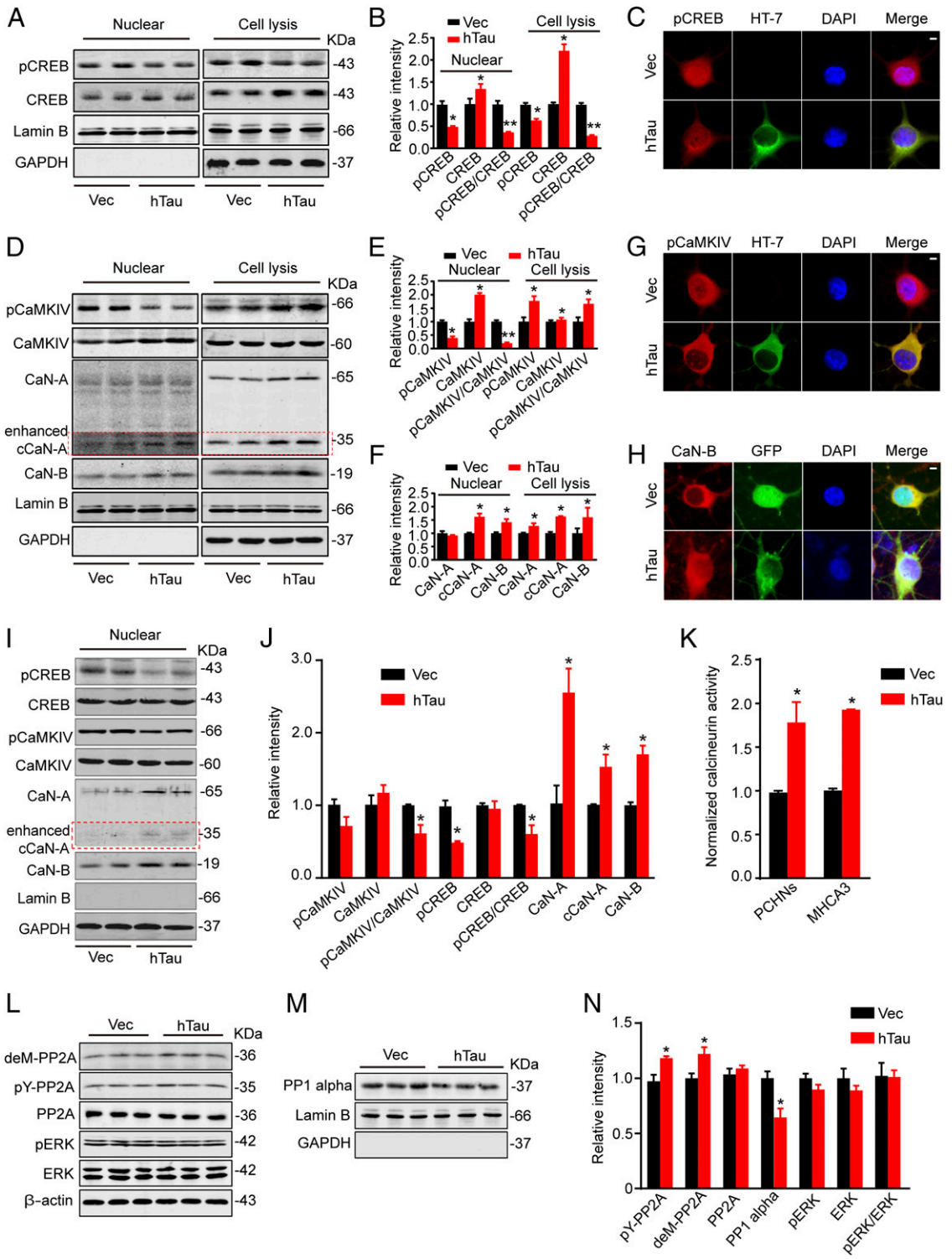

Fig. 3. Overexpression of hTau inactivates nuclear CREB with up-regulation of CaN and inhibition of CaMKIV. (*A* and *B*) Hippocampal neurons (7 div) were infected with lenti-mCherry-hTau or the vector and cultured for 5 more days, then the cell lysates and the nuclear fraction were prepared for Western blotting of total and the Ser133-phosphorylated levels of CREB. (*C*) The representative immunofluorescence imaging showing reduced nuclear staining of pCREB (red) in neurons with overexpression of hTau probed by HT7 (green). (Scale bar, 5 μm.) (*D–F*) The protein levels of total and the pCaMKIV, total CaN-A and CaN-B, and the cleaved CaN-A (cCaN-A) in cell lysates and the nuclear fraction detected by Western blotting. (*G* and *H*) The reduced pCaMKIV (red) and increased CaN-B (red) in the nuclear fraction of the primary hippocampal neurons detected by immunofluorescent staining. (Scale bar, 5 μm.) (*I* and *J*) The increased protein levels of CaN-A and cCaN-A, CaN-B, and reduced pCaMKIV and pCREB detected in nuclear fraction of the hippocampal CA3 subset after infusion of AAV-eGFP-hTau for 6 wk. (*K*) The CaN activity in primary cultured hippocampal neurons (PCHNs) and mouse hippocampus CA3 (MHCA3) detected by using the activity assay kit. (*L–N*) Total PP2A, the demethylated PP2A at Leu309 (deML309-PP2A), and the phosphorylated PP2A at tyrosine-307 (pY307-PP2A), total ERK, and pERK in cell lysates, and the level of PP1 catalytic subunit in the nuclear fraction measured by Western blotting. Lamin B and DAPI were used, respectively, as nuclear markers. Data were expressed as mean ± SEM, $*P < 0.05$, $**P < 0.01$ vs. Vec.

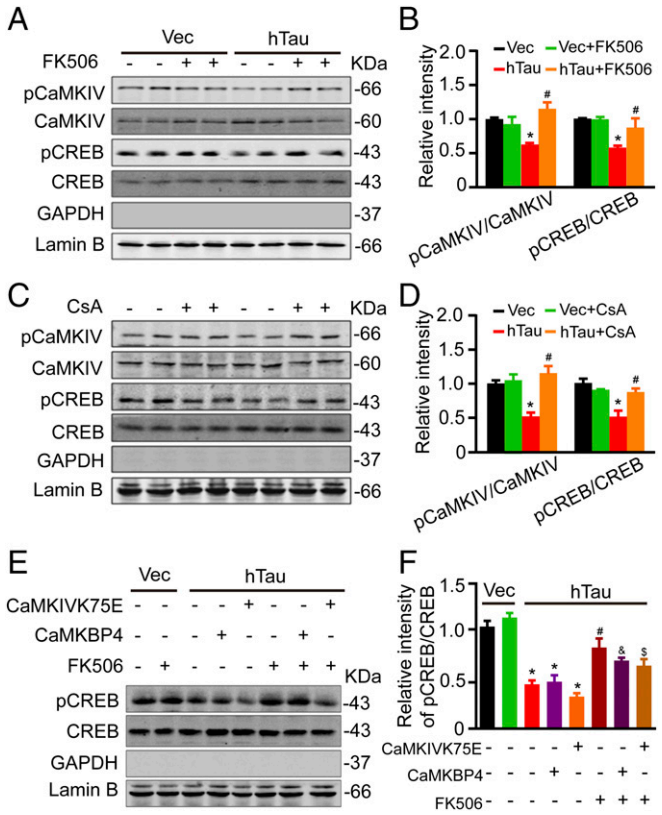

Fig. 4. Inhibition of CaN attenuates the hTau-induced CREB dephosphorylation independent of its effects on CaMKIV inhibition. (*A–D*) The primary hippocampal neurons (7 div) were infected with lenti-mCherry-hTau or the vector, after being cultured for 5 more days, the neurons were treated with 1 μM FK506 or 50 nM CsA for 12 h, then the levels pS133-CREB and pS196-CaMKIV were measured by Western blotting. (*E* and *F*) N2A cells, cotransfected with hTau plus CaMKBP4 or CaMKIVK75E plasmids for 48 h, were treated with 1 μM FK506 for 12 h, and then the phosphorylation level of CREB in the nuclear fraction was measured by Western blotting. Data were expressed as mean ± SEM, $^{*}P < 0.05$ vs. Vec; $^{\#}P < 0.05$ vs. hTau; and $^{\&}P < 0.05$ vs. hTau plus CaMKBP4; $^{\$}P < 0.05$ vs. hTau plus CaMKIVK75E.

of sEPSCs (Fig. 5 *H* and *I*), the IO curve (Fig. 5*J*) and the fEPSP slope in long-term potentiation (LTP) (Fig. 5 *K* and *L*) with restoration of spine density in hippocampal CA3 (Fig. 5 *M* and *N*). These data confirm the role of CaN activation in mediating hTau-induced synaptic toxicity and in memory deficits.

Discussion

As abnormal tau is the major proteinaceous component of neurofibrillary tangles in AD neurons, previous studies have been focused on exploring the upstream factor that can cause abnormal posttranslational modifications of tau, such as hyperphosphorylation (44). However, these studies cannot provide a satisfying answer to address the very chronic progression of AD pathologies, even in the absence of the original causes. We speculate that tau accumulation per se may serve as a cause to initiate a vicious circle of neurodegeneration. By overexpression of hTau to mimic intraneuronal tau accumulation as seen in the majority of AD cases, we demonstrated in the present study that intracellular accumulation of human wild-type full-length tau activated CaN and thus dephosphorylated/inactivated nuclear CaMKIV/CREB signaling, eventually resulting in synapse and memory impairments. We further demonstrated that the hTau-induced CaN activation can dephosphorylate CREB independent of CaMKIV inactivation, and simultaneous down-regulation of CaN efficiently rescues hTau-induced synapse and memory deficits. Our findings reveal a new mechanism to link intracellular hTau accumulation with chronic memory deterioration, implying that CaN may serve as a potential target for arresting tauopathies.

CaN is an autoinhibitory Ca^{2+}/calmodulin-dependent protein phosphatase highly enriched in the central nervous system. Structurally, CaN is composed of a catalytic A subunit and a Ca^{2+}-binding B subunit. Following Ca^{2+} binding, the autoinhibition is alleviated and the enzyme is activated (45). From previous studies, some show reduction or no change in protein level or the activity of CaN in AD or aging brains (33, 46–48), whereas others report that CaN is activated in AD brains (49, 50). Because CaN can dephosphorylate abnormally hyperphosphorylated tau proteins, activation of CaN should be beneficial for AD-like tau pathologies. On the other hand, it was also reported that activation of CaN by Aβ induced spine loss, dystrophic neurites, and dendritic simplification (51). These data suggest a complicated function of CaN, which may be clarified in future studies. Additionally, CaN A subunit (~56 kDa) can be truncated into shorter fragments (~40 kDa and ~48 kDa) by calpain-1 or caspase-3 or Aβ, and truncation increases the activity of phosphatase (52, 53). We also detected an increased cleavage of CaN A and B subunits with increased phosphatase activity in the current study. CaN may accelerate PP1-mediated CREB dephosphorylation (54, 55). Whereas our data show decreased PP1α in the nuclear fraction, which excludes the involvement of PP1α in hTau-induced CREB dephosphorylation. Because CaN is downstream of the altered intracellular calcium concentration (56), we speculate that hTau accumulation may activate CaN by perturbing calcium homeostasis.

We notice that phosphorylation of CaMKIV was significantly up-regulated in total lysates, but the level of pCaMKIV in the nuclear fraction was much lower in the hTau-expressing neurons than the vector controls, which suggests an impaired nuclear translocation and/or a reduced phosphorylation of CaMKIV in the nuclei. As a key regulator of neuronal gene expression, phosphorylation of CaMKIV by Ca^{2+}/CaM increases the activity and promotes the nuclear translocation of CaMKIV (57). Upon phosphorylation, the catalytically active CaMKIV gains access to the nuclei where it activates CREB-dependent gene expression (58, 59). The nuclear translocation of CaMKIV is also regulated by importin-α (60). In hippocampal neurons, CaMKIV has a predominant nuclear localization where it mediates distinct features of basal and activity-dependent dendrite complexity (61, 62). It was also reported that both PP2A and CaN can dephosphorylate CaMKIV (28, 63). Our data show that PP2A was inhibited and CaN was activated in the nuclear fraction upon overexpression of hTau, which excludes the role of PP2A in hTau-induced CaMKIV dephosphorylation. Therefore, the reduction of nuclear pCaMKIV observed in the current study can result from activation of CaN or an impaired nuclear translation of pCaMKIV induced by hTau accumulation.

Previous studies have shown that overexpression of P301L mutant tau impairs dendrites (64); we found in the current study that overexpression of wild-type human tau, as seen in the majority of sporadic AD, also results in spine loss and dendritic simplification in primarily cultured hippocampal neurons and in mouse brains. Tau may interact directly with postsynaptic signaling complexes, regulate glutamatergic receptor content in dendritic spines (65), and influence targeting and function of synaptic mitochondria (66, 67). Tau-targeted immunotherapy can reduce tau pathologies and synapse loss (68), indicating that the toxic effects of tau may be reversible. Therefore, understanding the role of tau in degenerating synapses is crucial for the development of therapeutic strategies designed to ameliorate synapse loss and preserve memory capacities.

Accumulation of wild-type tau is the hallmark of sporadic AD, which accounts for over 95% of AD cases. In autopsied AD brain tissue and cerebrospinal fluid, tau protein was increased by

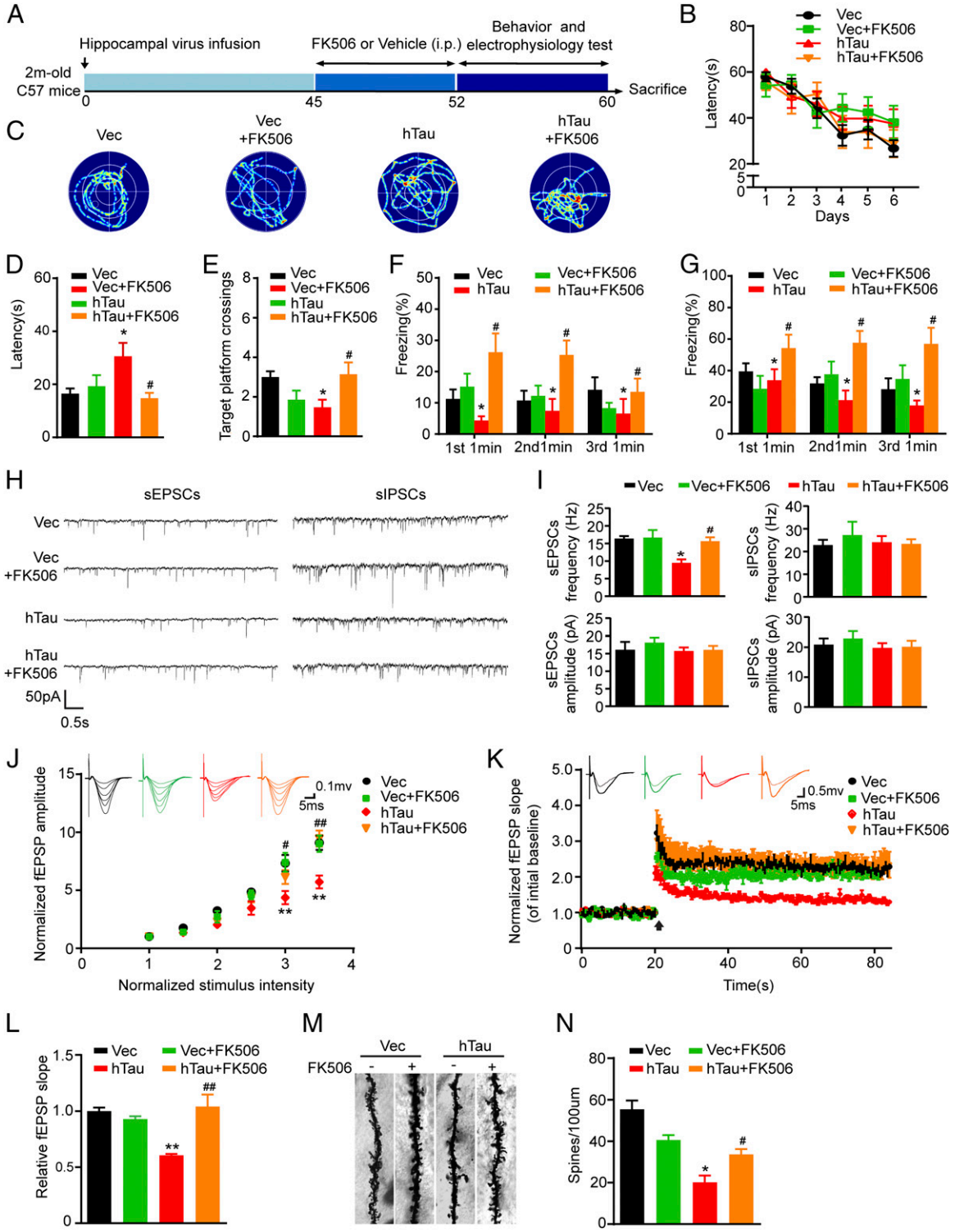

Fig. 5. Inhibition of CaN rescues the hTau-induced memory deficits with improvement of dendritic plasticity and synaptic functions. (*A*) Schematics show the treatments. AAV-eGFP (Vec) or AAV-eGFP-hTau (hTau) was injected stereotaxically into the hippocampal CA3 of 2-mo-old mice. After 45 d, FK506 (10 mg·kg·d) or the vehicle was injected intraperitoneally for 1 wk. Then the cognitive behaviors and synaptic plasticity were detected. (*B*) The escape latency to find the hidden platform during the 6-d learning process in MWM test. (*C*) The representative swimming tracks during the memory test carried out on day 8 by removing the hidden platform. (*D* and *E*) The escape latency to find the platform and target platform crossings tested on day 8. (*F* and *G*) Fear conditioning was used to measure the contextual memory of the mice 1 wk after the last MWM task. (*H*) The representative traces of sEPSCs and sIPSCs recorded by whole-cell voltage patch-clamp on ex vivo brain slices after FK506 or vehicle treatment. (*I*) The average frequency and amplitude of sEPSCs or sIPSCs collected from at least 12 neurons per group. (Scale bars, 10 pA, 1 s.) (*J*) The IO curve of fEPSP recorded on acute hippocampal slices overexpressing hTau or the vector and treated with FK506 or the vehicle ($n = 6$ per group). (*K*) The slope of fEPSP after HFS recorded on hippocampal slices after FK506 or vehicle treatment ($n = 6$ per group). Arrow indicates HFS onset, the average traces fEPSPs before (thin) and after (thick) LTP induction are shown. (*L*) Quantitative analyses for normalized fEPSPs 60–80 min after HFS. (*M* and *N*) The spine density in hippocampal CA3 subset imaged by Golgi staining. The data were expressed as mean ± SEM, $^{*}P < 0.05$, $^{**}P < 0.01$, Vec vs. hTau; $^{\#}P < 0.05$, $^{\#\#}P < 0.01$, hTau vs. hTau plus FK506.

approximately three- to eightfold of control level (69–71). Therefore, the AAV-delivered robust overexpression of tau in neurons as seen in the current study can mimic AD-like intracellular tau accumulation. Nonetheless, the levels of intracellular tau accumulation should be variable at different stages of the disease progression and at different brain regions or even in different types of neural cells. A dose-dependent intracellular tau accumulation was seen by exogenous transfection (72), which allowed the precise identification of the pathophysiological role of tau.

It is well recognized that tau abnormality plays a pivotal role in neurodegeneration. As a cytoskeleton protein, how tau accumulation induces neurodegeneration is not clear. One of the major findings in the present study is that hTau accumulation dephosphorylates/inactivates CREB. CREB is an important transcription factor and CREB inactivation leads to the inhibition of many promoter-containing CREs, including synaptic proteins and neurotrophic factors. Therefore, tau accumulation may induce neurodegeneration by inhibiting CREB. The most recognized function of tau is to promote microtubule assembly and maintain the stability of the microtubules. Intracellular accumulation of tau can block axonal transport, which can also contribute to the hTau-elicited molecular changes. These interesting issues deserve further investigation.

Together, we find in the present study that intracellular accumulation of hTau causes synapse and memory deficits through CaN-mediated dephosphorylation/inactivation of CaMKIV/CREB signaling in the nuclei.

Materials and Methods

Plasmids, Viruses, and Reagents. The plasmid pEGFP-tau-2N4R, encoding hTau, was a generous gift from Fei Liu (Jiangsu Key Laboratory of Neuroregeneration, Nantong University, Nantong, China). Based on it, DsRed-tau-2N4R, AAV-CAG-eGFP-hTau, and lentivirus CMV-mCherry-hTau were constructed and packaged as previously described in our laboratory (73, 74). CaMKBP4 and CaMKIVK75E plasmids were generous gifts from Tian-ming Gao (Southern Medical University, Guangzhou, China). All plasmids were sequenced and prepared using an endotoxin-free plasmid extraction kit (Tiangen). Lipofectamine 3000 transfection reagents were from Invitrogen. Multiplicity of infection (MOI 10) was used for virus infection in vitro and in vivo. The calcineurin inhibitors (FK506 and cyclosporine A) were from Tocris. All other reagents were obtained from Sigma-Aldrich.

Animals, Stereotaxic Surgery, and Drug Treatment. Male c57bl/6 mice (2-mo-old, 100 ± 20 g), supplied by the Experimental Animal Central of Wuhan University, were kept with accessible food and water under a 12-h light/dark cycle. All animal experiments were approved by the Ethics Committee of Tongji Medical College. Mice were anesthetized with 6% (wt/vol) chloral hydrate (300 mg/kg) and placed in a stereotaxic apparatus. After being sterilized with iodophors and 75% (vol/vol) alcohol, the scalp was incised along the midline between the ears. Holes were drilled in the hibateral skull stereotaxically at posterior 2.2 mm, lateral 2.7 mm, and ventral 2.3 mm relative to bregma. Using a microinjection system (World Precision Instruments), AAV-CAG-eGFP-hTau or vector (1 μL, 3.78×10^{12} viral genomes per milliliter) was injected in the hippocampus CA3 region at a rate of 0.125 μL/min, the needle was kept in place for 10 min before withdrawal, the skin was sutured, and the mice were placed beside a heater for analepsia. FK506 (Astellas Ireland) dissolved in 100% ethanol (10 mg/mL stock solution) was stored at −20 °C. Before injection, the FK506 was diluted to 2 mg/mL with sterile 0.9% saline containing 5% (vol/vol) Tween-80 and 5% (vol/vol) PEG-400. At 6 wk after brain infusion of the virus, FK506 was injected intraperitoneally (10 mg/kg) daily for 7 d.

MWM. Spatial learning and memory were tested by MWM as described in a previous study (75). For spatial learning, the mice were trained in the water maze to find a hidden platform for 6 consecutive days, four trials per day (with a 30-min interval) from 2:00 PM to 8:00 PM. In each trial, the mouse started from one of four quadrants facing the wall of the pool and ended when the animal climbed on the platform. If the mice did not locate the platform in 60 s, they were guided to the platform. The swimming path and the time used to find the platform (latency) was recorded by a video camera fixed to the ceiling of the room, 1.5 m from the water surface. Spatial memory was tested 2 d (day 8) after training. The platform was removed and the percentage of time spent in the target quadrant and the number of platform crossings were recorded.

Fear Conditioning. Fear conditioning was carried out as described previously (32, 76). Mice were placed into a square chamber with a grid floor. On the first day (day 1), each mouse was habituated to the chamber for 3 min, and then an auditory cue was delivered (70 dB, 30 s) followed by a foot shock (0.8 mA, 2 s). Then the mice were returned to their home cages. The same procedure was repeated two times with 2-min intervals. On the next day (day 2), the mice were exposed to the same chamber without any stimulus for 3 min. The contextual conditioning was assessed by recording freezing behavior during the 3-min exposure. After 2 h, the mice were put into the same chamber for 3 min followed by a 30-s auditory cue; freezing time during the 3 min was recorded for assessment of memory.

Electrophysiological Recordings. Mice (2 mo old) were used for all our electrophysiology experiments. Mice were deeply anesthetized as mentioned above. When all pedal reflexes were abolished, brains were removed and placed in ice-cold oxygenated slicing solution containing the following: 225 mM sucrose, 3 mM KCl, 1.25 mM NaH_2PO_4, 24 mM $NaHCO_3$, 6 mM $MgSO_4$, 0.5 mM $CaCl_2$, and 10 mM D-glucose. Coronal slices (350-μm thick) containing the dorsal hippocampus were cut at 4–5 °C in the slicing solution using a Leica VT1000S vibratome and then transferred to an incubation chamber filled with oxygenated slicing solution in a 30 °C water bath for 1 h before being recorded.

For LTP, slices were laid down in a chamber with an 8 × 8 microelectrode array in the bottom planar (each 50 × 50 μm in size, with an interpolar distance of 150 μm) and kept submerged in artificial cerebrospinal fluid (aCSF; 1–2 mL/min) with a platinum ring glued by a nylon silk. Signals were acquired using the MED64 System (Alpha MED Sciences, Panasonic). The fEPSPs in CA1 neurons were recorded by stimulating the Schaeffer fibers from CA3. LTP was induced by applying three trains of high-frequency stimulation (HFS; 100 Hz, 1-s duration).

For sEPSCs and sIPSCs, whole-cell recordings were performed using a Multiclamp 700B amplifier. Data were digitized with a Digidata 1440 and analyzed by pClamp 10.0 (Molecular Devices). The whole-cell currents were filtered at 5 kHz with a low-pass Bessel filter and digitized at between 5 and 20 kHz. Neurons of the hippocampus CA3 region were visualized for whole-cell recording and a pipette with a resistance of 3–5 MΩ. Recordings were conducted in a submerged recording chamber perfused (2–3 mL/min) with the aCSF: 126 mM NaCl, 3 mM KCl, 1.25 mM NaH_2PO_4, 24 mM $NaHCO_3$, 2 mM $MgSO_4$, 2 mM $CaCl_2$, and 10 mM glucose, equilibrated with 95% O_2 and 5% CO_2 at room temperature. Series resistance (<20 MΩ) or membrane resistance (300–500 MΩ) was monitored throughout the whole-cell recording and data were discarded if the resistance changed by more than 20%. For recording of sEPSCs, electrodes were filled with: 125 mM K-gluconate, 13 mM KCl, 10 mM Hepes, 10 mM EGTA, 2 mM MgATP, and 5 mM QX-314 bromide (pH 7.2 with KOH). The sEPSCs were recorded using a voltage-clamp at a holding potential of −70 mV. A total of 10 μM bicuculline methiodide was used to abrogate GABAA-mediated inhibitory synaptic activity. The sIPSCs were recorded at a holding potential of −70 mV. A CsCl-based internal solution also was used to enhance GABA-mediated currents, containing: 120 mM CsCl, 30 mM Hepes, 0.2 mM EGTA, 2 mM $MgCl_2$, 1 mM $CaCl_2$, 4 mM MgATP, and 5 mM QX-314 bromide. The experiments were conducted with DL-2-amino-5-phosphonopentanoic acid (AP5, 50 μM) and 6,7-dinitroquinoxaline-2,3-dione (DNQX, 10 μM) to block any glutamatergic synaptic events.

Primary Hippocampal Neuron Culture. Primary hippocampus neurons were prepared from 17- to 18-d-old rat embryos. Hippocampus were dissected and gently minced in Hank's buffered saline solution, then suspended in 0.25% (vol/vol) trypsin solution at 37 °C for 15 min. Neurons were plated in culture dishes coated with 100 μg/mL poly-D-lysine and cultured for 7 div in neurobasal medium supplemented with 2% (vol/vol) B-27 and 1× GlutaMAX for plasmid transfection and lentivirus infection. All cell culture reagents were purchased from Thermo Fisher Scientific.

Dendrite Length and Spine Analyses. For assessment of neuron morphology and spine density (77), hippocampal neurons were cotransfected with eGFP and dsRed or dsRed-hTau plasmids at 7 div using Lipofectamine 3000 according to the manufacturer's instruction, and then fixed in 4% (wt/vol) paraformaldehyde and 4% (wt/vol) sucrose buffer for 10 min at 12 div. A *z* stack of the optical section was captured using Carl Zeiss LSM710 confocal microscope with 100× oil objective. At least 30 neurons from three batches

of cultures were used for quantitative analysis per group by Image-Pro Plus 6.0 software.

The dendrite length was analyzed as previously described (78). The hippocampal neurons (7 div) were infected with lenti-mCherry-hTau or the control virus, after being cultured for another 5 d, and the neurons were fixed in 4% (wt/vol) paraformaldehyde, and then incubated with mouse monoclonal MAP2 antibody (1:1,000; Sigma, M4403) at 4 °C overnight. The neurons were washed in PBS and incubated with donkey anti-mouse Alexa-Fluor 488 secondary antibody (1:1,000; Invitrogen, A-21202) at room temperature for 1 h. Images were captured using a Carl Zeiss LSM710 confocal microscope. At least 50 cultured neurons from three different cultures were used for quantitative analysis per group using Image-Pro Plus 6.0 software by the single-blind method.

CaN Activity Assay. The activity of CaN was assayed by using a calcineurin cellular activity assay kit (207007, Millipore) by following the manufacturer's instructions.

Immunoprecipitation. The dissected hippocampal CA3 tissue was homogenized on ice in lysis buffer [50 mM Tris·HCl pH 8.0, 150 mM NaCl, 1% (vol/vol) Triton X-100, 1 mM EDTA, 1 mM $MgCl_2$, 10% (vol/vol) glycerol, 1:100 PMSF, 1:1,000 protease inhibitor mixture containing 4-(2-Aminoethyl)-benzenesulfonyl fluoride hydrochloride, aprotinin, bestatin, leupeptin, E-64, and pepstatin A] at 4 °C for 30 min, centrifugated at 12,000 × *g* for 10 min as described previously. A total of 200 μL supernatants containing about 200 μg total proteins were incubated at 4 °C overnight on rotation at 4 °C with 2 μg anti-NFATc4 antibody followed by the addition of protein A + G agarose at 4 °C for 2 h. The agarose beads were washed three times and resuspended in 50 μL of sample buffer containing 50 mM Tris·HCl, pH 7.6, 2% (wt/vol) SDS, 10% (vol/vol) glycerol, 10 mM DTT, 0.2% (wt/vol) bromophenol blue, and then denatured at 95 °C for 10 min (79). Immunoprecipitates were analyzed by Western blotting with antiphosphoserine/threonine antibodies.

Western Blotting. Western blotting was performed by the methods established in our laboratory (43). Briefly, for preparation of total cell extracts, the dissected hippocampal CA3 tissue or 12 div primary hippocampal neurons were homogenized or lysed in RIPA buffer and then centrifuged at 5,000 × *g* for 10 min, and the supernatant was collected and the protein levels were analyzed. The nuclear fraction was prepared by using the NE-PER Nuclear and Cytoplasmic Extraction kit (Pierce) following the manufacturer's instructions. The proteins in the extracts were separated by SDS/PAGE and analyzed by Western blotting using antibodies against pCREB (1:500; Cell Signaling, 9181), CREB (1:500; Cell Signaling, 9197), pCaMKIV (1:500; Santa Cruz, sc-28443), CaMKIV (1:500; Santa Cruz, sc-136249), γCaMKII (1:1,000; Santa Cruz, sc-1541), CaMKII (1:500; Cell Signaling, 3362), pCaMKII-α (1:500; 3361), pS9GSK-3β (1:500; Cell Signaling, 9323), GSK-3β (1:500; Santa Cruz, sc-8257), NFATc4 (1:250; Santa Cruz, sc-13036), phosphoserine/threonine (1:500; Abcam, ab17464), CaN-A (1:500; Santa Cruz, sc-9070), CaN-B (1:1,000; Millipore, 07–069), pERK1/2 (1:1,000; Cell Signaling, 4370), p-PP2A-Y307 (1:1,000; Abcam, ab32104), dem-PP2AC (1:1,000; Millipore, 05–577), HT-7 (1:1,000; Thermo Fisher, MN1000), DM1A (1:1,000; Sigma, T9026), Lamin-B1(1:1,000; Abcam, ab16048), GAPHD (1:1,000; Abcam, ab9482), and β-actin (1:1,000; Abcam, ab6272). Membranes were then incubated with a secondary antibody (1:10,000; Odessey) at room temperature. Immunoreactive bands were visualized with the Odyssey Infrared Imaging System (Li-Cor Biosciences) and quantitatively analyzed by ImageJ software.

Immunofluorescence. Cultured neurons were fixed in 4% (vol/vol) paraformaldehyde for 15 min and permeabilized in phosphate buffer containing 0.5% Triton X-100 (PBST). Nonspecific binding blocked incubating in PBST buffer containing 0.1% Triton X-100 and 5% (wt/vol) BSA for 1 h. The primary antibodies against pCREB (1:100), pCaMKIV (1:100), or CaN-B (1:100) were then applied in blocking solution and incubated at 4 °C overnight. The secondary antibodies conjugated to Alexa-Fluor 488/568 were added to the coverslip for 1 h at room temperature, and then DAPI (1:1,000) for 10 min. The coverslips were washed and mounted onto slides and imaged as previously described.

Statistical Analyses. Statistical analyses were performed by Student's *t* test for two-group comparisons, one-way or two-way ANOVA, followed by post hoc tests for multiple comparisons among more than two groups. The results were presented as mean ± SEM and $P < 0.05$ was accepted as statistically significant.

ACKNOWLEDGMENTS. We thank Dr. Fei Liu (Jiangsu Key Laboratory of Neuroregeneration) for the EGFP-hTau plasmid, and Dr. Tian-ming Gao (Southern Medical University) for CaMKBP4 and CaMKIVK75E plasmids. This study was supported in part by the Natural Science Foundation of China (Grants 81528007, 81171195, 81261120570, and 91132305) and by the Ministry of Science and Technology of China (Grant 2013DFG32670).

1. Bennett DA, Schneider JA, Bienias JL, Evans DA, Wilson RS (2005) Mild cognitive impairment is related to Alzheimer disease pathology and cerebral infarctions. *Neurology* 64(5):834–841.
2. Glenner GG, Wong CW (1984) Alzheimer's disease: Initial report of the purification and characterization of a novel cerebrovascular amyloid protein. *Biochem Biophys Res Commun* 120(3):885–890.
3. Grundke-Iqbal I, et al. (1986) Microtubule-associated protein tau. A component of Alzheimer paired helical filaments. *J Biol Chem* 261(13):6084–6089.
4. Davies CA, Mann DM, Sumpter PQ, Yates PO (1987) A quantitative morphometric analysis of the neuronal and synaptic content of the frontal and temporal cortex in patients with Alzheimer's disease. *J Neurol Sci* 78(2):151–164.
5. DeKosky ST, Scheff SW (1990) Synapse loss in frontal cortex biopsies in Alzheimer's disease: Correlation with cognitive severity. *Ann Neurol* 27(5):457–464.
6. Thal DR, et al. (2000) Alzheimer-related tau-pathology in the perforant path target zone and in the hippocampal stratum oriens and radiatum correlates with onset and degree of dementia. *Exp Neurol* 163(1):98–110.
7. Rapoport M, Dawson HN, Binder LI, Vitek MP, Ferreira A (2002) Tau is essential to beta-amyloid-induced neurotoxicity. *Proc Natl Acad Sci USA* 99(9):6364–6369.
8. Scheff SW, Price DA, Schmitt FA, DeKosky ST, Mufson EJ (2007) Synaptic alterations in CA1 in mild Alzheimer disease and mild cognitive impairment. *Neurology* 68(18): 1501–1508.
9. Terry RD, et al. (1991) Physical basis of cognitive alterations in Alzheimer's disease: Synapse loss is the major correlate of cognitive impairment. *Ann Neurol* 30(4): 572–580.
10. Frankfurt M, Luine V (2015) The evolving role of dendritic spines and memory: Interaction(s) with estradiol. *Horm Behav* 74:28–36.
11. Lue LF, et al. (1999) Soluble amyloid beta peptide concentration as a predictor of synaptic change in Alzheimer's disease. *Am J Pathol* 155(3):853–862.
12. Polydoro M, Acker CM, Duff K, Castillo PE, Davies P (2009) Age-dependent impairment of cognitive and synaptic function in the htau mouse model of tau pathology. *J Neurosci* 29(34):10741–10749.
13. Yoshiyama Y, et al. (2007) Synapse loss and microglial activation precede tangles in a P301S tauopathy mouse model. *Neuron* 53(3):337–351.
14. Sydow A, et al. (2011) Tau-induced defects in synaptic plasticity, learning, and memory are reversible in transgenic mice after switching off the toxic Tau mutant. *J Neurosci* 31(7):2511–2525.
15. Roberson ED, et al. (2007) Reducing endogenous tau ameliorates amyloid beta-induced deficits in an Alzheimer's disease mouse model. *Science* 316(5825):750–754.
16. Perazzona B, Isabel G, Preat T, Davis RL (2004) The role of cAMP response element-binding protein in *Drosophila* long-term memory. *J Neurosci* 24(40):8823–8828.
17. Bourtchuladze R, et al. (1994) Deficient long-term memory in mice with a targeted mutation of the cAMP-responsive element-binding protein. *Cell* 79(1):59–68.
18. Balschun D, et al. (2003) Does cAMP response element-binding protein have a pivotal role in hippocampal synaptic plasticity and hippocampus-dependent memory? *J Neurosci* 23(15):6304–6314.
19. Barco A, Alarcon JM, Kandel ER (2002) Expression of constitutively active CREB protein facilitates the late phase of long-term potentiation by enhancing synaptic capture. *Cell* 108(5):689–703.
20. Hardingham GE, Arnold FJ, Bading H (2001) Nuclear calcium signaling controls CREB-mediated gene expression triggered by synaptic activity. *Nat Neurosci* 4(3):261–267.
21. Yamamoto-Sasaki M, Ozawa H, Saito T, Rösler M, Riederer P (1999) Impaired phosphorylation of cyclic AMP response element binding protein in the hippocampus of dementia of the Alzheimer type. *Brain Res* 824(2):300–303.
22. Mantamadiotis T, et al. (2002) Disruption of CREB function in brain leads to neurodegeneration. *Nat Genet* 31(1):47–54.
23. Dash PK, Karl KA, Colicos MA, Prywes R, Kandel ER (1991) cAMP response element-binding protein is activated by Ca2+/calmodulin- as well as cAMP-dependent protein kinase. *Proc Natl Acad Sci USA* 88(11):5061–5065.
24. Xing J, Ginty DD, Greenberg ME (1996) Coupling of the RAS-MAPK pathway to gene activation by RSK2, a growth factor-regulated CREB kinase. *Science* 273(5277): 959–963.
25. Pende M, et al. (1997) Neurotransmitter- and growth factor-induced cAMP response element binding protein phosphorylation in glial cell progenitors: Role of calcium ions, protein kinase C, and mitogen-activated protein kinase/ribosomal S6 kinase pathway. *J Neurosci* 17(4):1291–1301.
26. Roberson ED, et al. (1999) The mitogen-activated protein kinase cascade couples PKA and PKC to cAMP response element binding protein phosphorylation in area CA1 of hippocampus. *J Neurosci* 19(11):4337–4348.
27. Sheng M, Thompson MA, Greenberg ME (1991) CREB: a Ca(2+)-regulated transcription factor phosphorylated by calmodulin-dependent kinases. *Science* 252(5011): 1427–1430.
28. Westphal RS, Coffee RL, Jr, Marotta A, Pelech SL, Wadzinski BE (1999) Identification of kinase-phosphatase signaling modules composed of p70 S6 kinase-protein phosphatase 2A (PP2A) and p21-activated kinase-PP2A. *J Biol Chem* 274(2):687–692.
29. Impey S, et al. (2002) Phosphorylation of CBP mediates transcriptional activation by neural activity and CaM kinase IV. *Neuron* 34(2):235–244.

30. Rebelo S, Santos M, Martins F, da Cruz e Silva EF, da Cruz e Silva OA (2015) Protein phosphatase 1 is a key player in nuclear events. *Cell Signal* 27(12):2589–2598.
31. Reese LC, Zhang W, Dineley KT, Kayed R, Taglialatela G (2008) Selective induction of calcineurin activity and signaling by oligomeric amyloid beta. *Aging Cell* 7(6):824–835.
32. Dineley KT, Hogan D, Zhang WR, Taglialatela G (2007) Acute inhibition of calcineurin restores associative learning and memory in Tg2576 APP transgenic mice. *Neurobiol Learn Mem* 88(2):217–224.
33. Lian Q, Ladner CJ, Magnuson D, Lee JM (2001) Selective changes of calcineurin (protein phosphatase 2B) activity in Alzheimer's disease cerebral cortex. *Exp Neurol* 167(1):158–165.
34. Tackenberg C, Brandt R (2009) Divergent pathways mediate spine alterations and cell death induced by amyloid-beta, wild-type tau, and R406W tau. *J Neurosci* 29(46): 14439–14450.
35. Benito E, Barco A (2010) CREB's control of intrinsic and synaptic plasticity: Implications for CREB-dependent memory models. *Trends Neurosci* 33(5):230–240.
36. Impey S, et al. (1998) Cross talk between ERK and PKA is required for Ca2+ stimulation of CREB-dependent transcription and ERK nuclear translocation. *Neuron* 21(4): 869–883.
37. Sun P, Enslen H, Myung PS, Maurer RA (1994) Differential activation of CREB by Ca^{2+}/calmodulin-dependent protein kinases type II and type IV involves phosphorylation of a site that negatively regulates activity. *Genes Dev* 8(21):2527–2539.
38. Ma H, et al. (2014) γCaMKII shuttles Ca^{2+}/CaM to the nucleus to trigger CREB phosphorylation and gene expression. *Cell* 159(2):281–294.
39. Matthews RP, et al. (1994) Calcium/calmodulin-dependent protein kinase types II and IV differentially regulate CREB-dependent gene expression. *Mol Cell Biol* 14(9): 6107–6116.
40. Graef IA, et al. (2003) Neurotrophins and netrins require calcineurin/NFAT signaling to stimulate outgrowth of embryonic axons. *Cell* 113(5):657–670.
41. Lee YI, et al. (2005) Membrane depolarization induces the undulating phosphorylation/dephosphorylation of glycogen synthase kinase 3beta, and this dephosphorylation involves protein phosphatases 2A and 2B in SH-SY5Y human neuroblastoma cells. *J Biol Chem* 280(23):22044–22052.
42. Beals CR, Clipstone NA, Ho SN, Crabtree GR (1997) Nuclear localization of NF-ATc by a calcineurin-dependent, cyclosporin-sensitive intramolecular interaction. *Genes Dev* 11(7):824–834.
43. Li HL, et al. (2007) Phosphorylation of tau antagonizes apoptosis by stabilizing beta-catenin, a mechanism involved in Alzheimer's neurodegeneration. *Proc Natl Acad Sci USA* 104(9):3591–3596.
44. Kimura T, et al. (2007) Hyperphosphorylated tau in parahippocampal cortex impairs place learning in aged mice expressing wild-type human tau. *EMBO J* 26(24): 5143–5152.
45. Klee CB, Crouch TH, Krinks MH (1979) Calcineurin: A calcium- and calmodulin-binding protein of the nervous system. *Proc Natl Acad Sci USA* 76(12):6270–6273.
46. Billingsley ML, et al. (1994) Calcineurin immunoreactivity in Alzheimer's disease. *Exp Neurol* 126(2):178–184.
47. Ladner CJ, Czech J, Maurice J, Lorens SA, Lee JM (1996) Reduction of calcineurin enzymatic activity in Alzheimer's disease: Correlation with neuropathologic changes. *J Neuropathol Exp Neurol* 55(8):924–931.
48. Celsi F, et al. (2007) Beta-amyloid causes downregulation of calcineurin in neurons through induction of oxidative stress. *Neurobiol Dis* 26(2):342–352.
49. Liu F, et al. (2005) Truncation and activation of calcineurin A by calpain I in Alzheimer disease brain. *J Biol Chem* 280(45):37755–37762.
50. Qian W, et al. (2011) Activation of protein phosphatase 2B and hyperphosphorylation of Tau in Alzheimer's disease. *J Alzheimers Dis* 23(4):617–627.
51. Wu HY, et al. (2010) Amyloid beta induces the morphological neurodegenerative triad of spine loss, dendritic simplification, and neuritic dystrophies through calcineurin activation. *J Neurosci* 30(7):2636–2649.
52. Mohmmad Abdul H, Baig I, Levine H, 3rd, Guttmann RP, Norris CM (2011) Proteolysis of calcineurin is increased in human hippocampus during mild cognitive impairment and is stimulated by oligomeric Abeta in primary cell culture. *Aging Cell* 10(1): 103–113.
53. D'Amelio M, et al. (2011) Caspase-3 triggers early synaptic dysfunction in a mouse model of Alzheimer's disease. *Nat Neurosci* 14(1):69–76.
54. Chang KT, Berg DK (2001) Voltage-gated channels block nicotinic regulation of CREB phosphorylation and gene expression in neurons. *Neuron* 32(5):855–865.
55. Mulkey RM, Endo S, Shenolikar S, Malenka RC (1994) Involvement of a calcineurin/inhibitor-1 phosphatase cascade in hippocampal long-term depression. *Nature* 369(6480):486–488.
56. Ryeom S, Greenwald RJ, Sharpe AH, McKeon F (2003) The threshold pattern of calcineurin-dependent gene expression is altered by loss of the endogenous inhibitor calcipressin. *Nat Immunol* 4(9):874–881.
57. Enslen H, Tokumitsu H, Soderling TR (1995) Phosphorylation of CREB by CaM-kinase IV activated by CaM-kinase IV kinase. *Biochem Biophys Res Commun* 207(3): 1038–1043.
58. Walton MR, Dragunow I (2000) Is CREB a key to neuronal survival? *Trends Neurosci* 23(2):48–53.
59. Sée V, Boutillier AL, Bito H, Loeffler JP (2001) Calcium/calmodulin-dependent protein kinase type IV (CaMKIV) inhibits apoptosis induced by potassium deprivation in cerebellar granule neurons. *FASEB J* 15(1):134–144.
60. Kotera I, et al. (2005) Importin alpha transports CaMKIV to the nucleus without utilizing importin beta. *EMBO J* 24(5):942–951.
61. Bito H, Deisseroth K, Tsien RW (1996) CREB phosphorylation and dephosphorylation: A Ca(2+)- and stimulus duration-dependent switch for hippocampal gene expression. *Cell* 87(7):1203–1214.
62. Nagendran T, Hardy LR (2011) Calcium/calmodulin-dependent protein kinase IV mediates distinct features of basal and activity-dependent dendrite complexity. *Neuroscience* 199:548–562.
63. Kasahara J, Fukunaga K, Miyamoto E (1999) Differential effects of a calcineurin inhibitor on glutamate-induced phosphorylation of Ca2+/calmodulin-dependent protein kinases in cultured rat hippocampal neurons. *J Biol Chem* 274(13):9061–9067.
64. Ramsden M, et al. (2005) Age-dependent neurofibrillary tangle formation, neuron loss, and memory impairment in a mouse model of human tauopathy (P301L). *J Neurosci* 25(46):10637–10647.
65. Miller EC, et al. (2014) Tau phosphorylation and tau mislocalization mediate soluble Aβ oligomer-induced AMPA glutamate receptor signaling deficits. *Eur J Neurosci* 39(7):1214–1224.
66. Amadoro G, et al. (2010) A NH2 tau fragment targets neuronal mitochondria at AD synapses: Possible implications for neurodegeneration. *J Alzheimers Dis* 21(2): 445–470.
67. Corsetti V, et al. (2015) NH2-truncated human tau induces deregulated mitophagy in neurons by aberrant recruitment of Parkin and UCHL-1: Implications in Alzheimer's disease. *Hum Mol Genet* 24(11):3058–3081.
68. Nakamura K, et al. (2012) Proline isomer-specific antibodies reveal the early pathogenic tau conformation in Alzheimer's disease. *Cell* 149(1):232–244.
69. Yamamori H, et al. (2007) Tau in cerebrospinal fluid: A sensitive sandwich enzyme-linked immunosorbent assay using tyramide signal amplification. *Neurosci Lett* 418(2):186–189.
70. Khatoon S, Grundke-Iqbal I, Iqbal K (1992) Brain levels of microtubule-associated protein tau are elevated in Alzheimer's disease: A radioimmuno-slot-blot assay for nanograms of the protein. *J Neurochem* 59(2):750–753.
71. Hu YY, et al. (2002) Levels of nonphosphorylated and phosphorylated tau in cerebrospinal fluid of Alzheimer's disease patients: An ultrasensitive bienzyme-substrate-recycle enzyme-linked immunosorbent assay. *Am J Pathol* 160(4):1269–1278.
72. Hu Y, et al. (2016) Tau accumulation impairs mitophagy via increasing mitochondrial membrane potential and reducing mitochondrial parkin. *Oncotarget* 7(14): 17356–17368.
73. Tiscornia G, Singer O, Verma IM (2006) Production and purification of lentiviral vectors. *Nat Protoc* 1(1):241–245.
74. Lemarchand P, et al. (1992) Adenovirus-mediated transfer of a recombinant human alpha 1-antitrypsin cDNA to human endothelial cells. *Proc Natl Acad Sci USA* 89(14): 6482–6486.
75. Peng CX, et al. (2013) Disease-modified glycogen synthase kinase-3β intervention by melatonin arrests the pathology and memory deficits in an Alzheimer's animal model. *Neurobiol Aging* 34(6):1555–1563.
76. Kass MD, Rosenthal MC, Pottackal J, McGann JP (2013) Fear learning enhances neural responses to threat-predictive sensory stimuli. *Science* 342(6164):1389–1392.
77. Hoover BR, et al. (2010) Tau mislocalization to dendritic spines mediates synaptic dysfunction independently of neurodegeneration. *Neuron* 68(6):1067–1081.
78. Ageta-Ishihara N, et al. (2013) Septins promote dendrite and axon development by negatively regulating microtubule stability via HDAC6-mediated deacetylation. *Nat Commun* 4:2532.
79. Luo HB, et al. (2014) SUMOylation at K340 inhibits tau degradation through deregulating its phosphorylation and ubiquitination. *Proc Natl Acad Sci USA* 111(46): 16586–16591.